



Research Article

Seismic evaluation of tall RC frames with hybrid friction damper and shape memory alloy designed by PBPD method

Faramarz Norouzi OJAEY¹, Heydar Dashti NASERABADI^{1,*}, Morteza JAMSHIDI¹

¹Department of Civil Engineering, Chalous Branch, Islamic Azad University, Chalous, 1477893855, Iran

ARTICLE INFO

Article history

Received: 19 September 2021

Revised: 09 November 2021

Accepted: 25 December 2021

Keywords:

Nonlinear Analysis; Opensees; Performance-Based Design; RC Frames; Shape Memory Alloy; Self-Centering

ABSTRACT

This paper suggests a novel lateral load-resisting solution for RC (high-rise reinforced concrete) frames using superelastic SMA wires as friction dampers. The suggested SMA-friction damper has some advantages, such as an easy-to-configure and affordable application, in addition to being able to control the frictional energy dissipation components mechanism in line with the design procedure based on the suggested effectiveness thanks to its self-centering SMA wires. With the least amount of SMA use, it may produce hysteretic behavior and an intense tendency for self-centering. The research used two distinct design modes—common and with the recommended damper—to construct two tall, 18- and 22-story RC frames. Ten far-field earthquakes were studied using OpenSees software in a nonlinear time history fashion. Eighteen and twenty-two-story reinforced concrete frame high-rises were designed in two distinct ways: normally and with the recommended damper. Aside from the major advancement in ductility, the lateral strength and stiffness gave an exceptional capacity for self-centering, resulting in a substantial decrease in most drift and persistent distortions in the structure. The study's findings showed that the suggested damper may improve the RC frame's structural performance while using the fewest bracing spans and money.

Cite this article as: Ojaey FN, Naserabadi HD, Jamshidi M. Seismic evaluation of tall RC frames with hybrid friction damper and shape memory alloy designed by PBPD method. Sigma J Eng Nat Sci 2024;42(6):1683–1696.

INTRODUCTION

The least amount of harm done to structural and non-structural systems occurs during mild earthquakes when standard seismic systems are used in concrete structures. However, the main seismic load-bearing members which are generally permanent members of their structural system should be replaced to create a strong resistance to future severe earthquakes. Because of this, using

a replacement hybrid passive control system in high-rise buildings becomes more crucial because it is neither practicable nor easy to implement in standard systems. One popular kind of non-permanent passive damper that is frequently used to regulate seismic activity in buildings is the friction damper, which is employed as an energy absorber in this work [1-3]. Instead of the primary parts of the building yielding non-ductilely during the powerful earthquake

*Corresponding author.

*E-mail address: dashti@iauc.ac.ir

This paper was recommended for publication in revised form by Editor-in-Chief Ahmet Selim Dalkilic



movements, friction equipment slides and dissipates a considerable portion of the vibrating energy into heat. Construction seismic behavior may be effectively improved with the use of hybrid friction dampers. It has a straightforward mechanism, is insensitive to temperature changes, and reduces earthquake energy by impacting friction.

While passive devices prevent damage to both structural and non-structural systems during seismic activity, their use frequently leaves significant and long-lasting residual deformation in the wake of a seismic event.

According to recent studies, it is preferable to rebuild a new structure rather than reconstruct or repair a damaged one when the ratio of residual drift is more than 0.5% [4]. Because the integrated structure is made of concrete elements, this is a significant drawback for RC structures. The moment-resistant method is chosen by the designer since the concrete shear wall system is impractical for controlling significant drifts, particularly in metropolitan locations with high-rise buildings adjacent to one another due to architectural needs for ventilation and illumination. For instance, following the Michoacán earthquake in 1985, the majority of the RC-damaged structures were demolished due to a significant, ongoing inter-story drift [5].

It is now necessary to design structures using a performance-based approach due to seismic concerns. As a result, new structural components and systems need to be more resilient to damage, capable of reversing or lessening irreversible deformations, and have better resilience to deformation.

Several investigations were created and evaluated for the SMAs application in civil engineering for devices with self-centering attributes [6-16]. Their efficacy in mitigating seismic activity within building structures has been demonstrated through numerical and experimental studies. Massah and Dorvar [17] looked at the impact of altering the hysteresis characteristics of SMA material, which was employed in eccentrically bracing frames as a passive control mechanism. According to the outcomes, using the SMA superelastic characteristic not only effectively increases ductility-stiffness and lateral resistance but also has great rehabilitation capacity. As a result, the structure's greatest thrust and residual distortions are significantly reduced. Qian and Song [1] looked into the effects of seismic stresses on a friction damper that had SMA installed. According to the findings, a friction damper fitted with a SMA significantly enhanced the structure's dynamic reaction during strong earthquakes by absorbing a noteworthy amount of the input energy. Moreover, the structure may be repurposed to take on additional seismic loads without any residual drift because of the damper's self-centering capability. Four distinct floors (3, 5, 7, and 9) of RC structures have been examined and exposed to near-field ground vibrations in the research given by Shiravand et al. [18]. Two types of reinforcement details are taken into consideration for each building: (1) RC frame (traditional steel reinforcement) and (2) SMA RC frame (steel-SMA reinforcement), where

steel bars are utilized in some areas and SMA bars in plastic zones of beams. The "SeismoStruct" finite element program has conducted nonlinear time history studies. Based on the findings, it can be concluded that using SMA materials in the areas where the beams have plastic hinges reduces residual displacement and, in turn, the need for post-quake repairs. Shape memory alloys are generally thought to minimize structural damage and retrofit expenses. It has been noticed that there is no discussion about how the plastic hinge regions are modeled in the Opensees software for selected 18 and 22-story reinforced concrete structure frames [19,20].

In this study, we want to identify a hybrid device that can dissipate energy and provide self-centering capability. The purpose of this device is to use performance-based plastic design methodologies to decrease residual deformation and increase seismic performance in high-rise moment-resistant frames. Due to the design approach, SMA wires have the maximum potential to restore the structure to its starting condition while also making the most significant contribution to the dissipation of energy in the friction damper. An additional technique for determining this objective is SMA trait evaluation. To study the potential uses of this kind of system for reinforced concrete (RC) buildings, an analysis of nonlinear time history is conducted on 18 and 22-story RC frames, both with and without the proposed hybrid damper.

MATERIALS AND METHODS

By focusing on its non-linear behavior, the PHFD (proposed hybrid friction damper) damper serves as a fuse inside the structure, preventing harm to other structural and non-structural elements as well as non-linear behavior. There are two components to the PHFD damper. The first part is a friction damper, which dissipates seismic energy by creating a perpendicular impact force between two contact plates using high-strength bolts. This type of damper frequently employs steel-on-brass, steel-on-steel, and brake pad layers on steel as sliding surfaces. The selection of a base metal is crucial for the operation of a friction damper. For the duration of the device, a high corrosion resistance might frequently lower the estimated friction reduction coefficient. The sliding surface characteristics of low-carbon steel alloys deteriorated over time due to rust and corrosion. There was no more corrosion observed in experiments conducted on stainless steel in contact with brass. Consequently, according to Lee et al. [21], these materials can be used as friction dampers. Friction dampers have their range of motion limited by slot holes that have slot lengths equal to S . Here, S denotes the highest degree of inter-story drift achievable at the specified efficiency level. The design strategy of the PHFD damper is centered on the objective of ensuring that the structure is constructed to resist the specified degree of seismic hazard. This construction prevents inter-story drift from exceeding the allowable

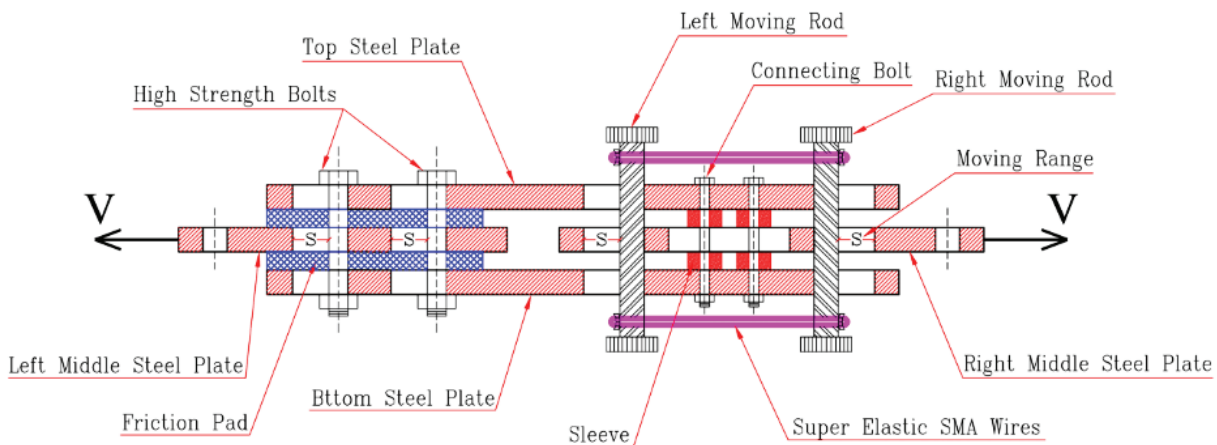


Figure 1. Configuration of the PHFD damper.

amount at the effectiveness level. The bolts crash into their end wall when the displacement hits S's sliding limit, at which point the motion cannot slip anymore.

This self-centering damper, which is built on super-elastic SMA wires, makes up the second half of the PHFD damper. The enormous force absorption and hysteric damping features of the superelastic NiTi wires are complemented by their quasi-self-centering function. The device can reduce the seismic reaction of a building and restore it to its pre-quake state by intelligently placing and modifying the number of superelastic SMA wires. This allows for energy dissipation and self-centering capacity. SMA cables circumscribe the two bars. This indicates that these two bars can travel on the right side's middle, lower, and higher steel plates by making a slot hole with a length of S. According to Figure 1, the tensile or compressive force range of each of these bars is identical, measuring S. The left bar is positioned S from the slot hole end, while the right bar is in contact with the slot hole at the beginning ($V = 0$). Due to the increase in frictional force and the SMA wires strengthening, the right rod moves to the right. However, the left bar remains stationary as the SMA wires continue to elongate. Eventually, the SMA wires will reach their maximum length and strength, causing the right middle steel plate to move even further until it collides with the left bar at the end of the slot hole. This research suggests that the design technique should find the optimal ratio of frictional force at the PHFD damper to SMA wires. Two dampers are ensured to work via coincidence, providing sufficient energy dissipation and self-centering capacity by seismic requirements.

Determination of the optimal ratio of SMA wires and friction damper

Relative to the ultimate friction damper force (V_F) and the inverted distortion yield force of SMA wires ($V_{SMA,r}$), the proposed hybrid damper's self-centering ability is mostly based on this relationship. The energy-absorbing

friction damper utilizes the tensile force, r , of V_{SMA} to apply it to SMA wires. This damper has a hysteresis loop that encompasses the whole range of strain and has a kinematic hardening value equivalent to 0% of the strain hardening ratio. This is caused by the loaded PHFD damper only deforming to the extent equivalent to Δr , or the deformation corresponding to the yield force of the inverted transformation of the SMA. In the meantime, the VF force-equipped friction damper dissipates energy, and the PHFD damper's total resistance becomes $V_{(SMA,r)} + V_F$. To clarify, for the PHFD damper to possess self-centering qualities and a flag-shaped hysteresis loop, the force $V_{SMA,r}$ has to align with the friction damper's ultimate yield force, as expressed in Eq. (1).

$$V_{SMA,r} \geq V_F \tag{1}$$

It should be noted that the maximum residual displacement of the PHFD damper ($\Delta_{residual}$) is simply equal to the yield drift of the reversed deformation of SMA as Eq. (2).

$$\Delta_{residue} = \Delta_r = \beta \epsilon_M^S L_{SMA} \tag{2}$$

Therefore, the value β for SMA wires is equivalent to the ratio of the forward transformation yield force ($V_{SMA,f}$) to the transformed evolution yield force ($V_{SMA,r}$).

The maximum movement of 1.5% of the floor height, which is calculated from the seismic design of the appropriate capability level, determines the length of the SMA wires. Since the secondary hardening phenomenon results in an unexpectedly large resistance, the strain restriction ϵ_M^S for SMA wires is meant to prohibit a reduction in their capacity to re-center themselves as well as minimize damage to nearby structural elements and friction dampers. But to avoid staying in the early austenitic phase of stiffness, too-long wires should be avoided. This means that Eq. (3) may be used to determine the length of the SMA wires.

$$L_{SMA} = \frac{\text{Drift}_{\text{allowable}} \times h_{\text{story}}}{\epsilon_M^C} \quad (3)$$

Where the power absorption friction damper exhibits kinematic stiffening with a non-zero strain strengthening rate, as illustrated in Figure 2, the friction damper resistance mustn't reach V_F until the load-deformation has reached Δ_r . The resistance difference between V_F and the friction damper resistance in Δ_r deformation during cyclic loading is called over resistance V_a and can be written as Eq. (4).

$$V_a = (\Delta_r - \Delta_{F,y}) S_F \quad (4)$$

Where, $\Delta_{F,y}$ and S_F are respectively equal to yield drift and the strain hardening for the friction damper. The overall resistance of the PHFD damper with the loading deformation of Δ_r is equal to $V_{SMA,r} + (V_F + V_a)$. Hence, the requirement for the PHFD damper is as Eq. (5).

$$V_{SMA,r} \geq V_F + V_a \quad (5)$$

It has been shown that the residual displacement of the PHFD damper rises as the addition strength of V_a increases. Hence, the calculated value of residual displacement for the PHFD damper is adjusted according to Equation (6).

$$\Delta_{\text{residue}} = \Delta_r + \frac{V_a}{S_F} \quad (6)$$

According to Eq. (6) it is known that the higher addition strength and the lower secondary stiffness of the PHFD damper can increase its residual deformation. Even so, the primary source of the PHFD damper's residual movement is still the inverse transformation yield drift of SMA. As a result, the self-centering capability of the PHFD damper is higher when the inverse transformation yield drift is reduced. Because of this, this section ignores the impact of the addition strength V_a .

Equation (7) defines the force distribution design between the self-centering Shape Memory Alloy (SMA) wires in the PHFD damper and the energy absorber friction damper. It relates the design yield force (V) with the ratio of β , stating that $V_{(SMA,r)}$ is equal to β times $V_{(SMA,f)}$.

$$\begin{aligned} V_{SMA,f} &\geq \frac{1}{1+\beta} V \\ V_F &\geq \frac{\beta}{1+\beta} V \end{aligned} \quad (7)$$

The necessary space for the SMA wire combination is obtained by finding the right balance between the required shear (V) for the PHFD damper model and the SMA rod setting tensile strength at a stress level of $\sigma_M^S=280$ MPa, as determined by Equation (8).

$$A_{SMA} \geq \frac{V_{SMA,f}}{\sigma_M^S} = \frac{V}{\sigma_M^S(1+\beta)} \quad (8)$$

Table 1 shows the distribution of shear force between SMA wires and friction damper in terms of different β values. It is found that increasing β will reduce the contribution

Table 1. The distribution of shear force between SMA wires and friction damper

β	SMA wires $\left(\frac{1}{1+\beta}\right)$ (%)	friction damper $\left(\frac{\beta}{1+\beta}\right)$ (%)
0.00	100.0	0.0
0.25	80.0	20.0
0.50	66.7	33.3
0.75	57.1	42.9
0.95	51.3	48.7
1.00	50.0	50.0

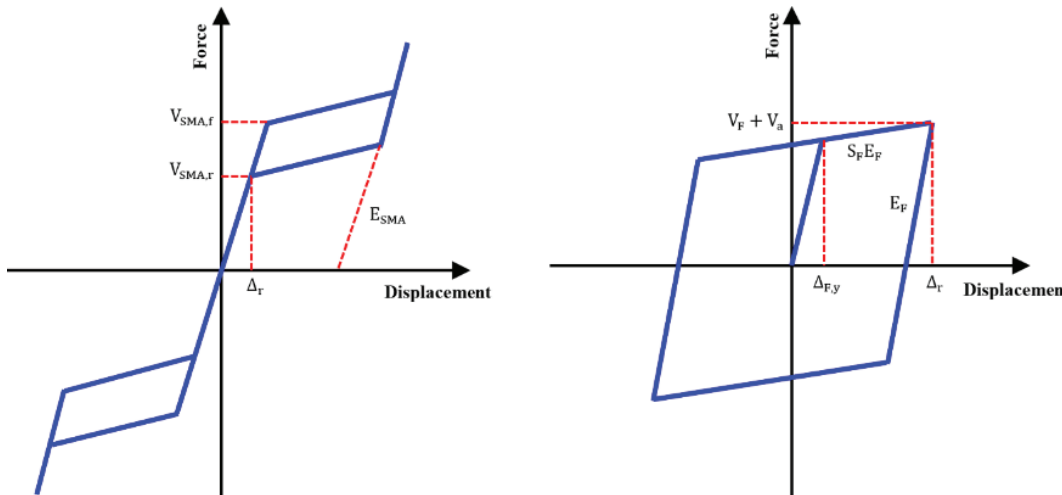


Figure 2. Hysteresis curve of SMA wires and friction damper.

of SMA wires in the shear force so that at the value $\beta = 0$, all the shear force is transferred to the SMA wires, and at the value $\beta = 1$, the shear force is evenly distributed between the friction damper and the SMA wires.

In this section, to determine the proposed design method for determining the optimal SMA wire ratio, for specific shear force of $V=300$ kN and different β values of 0.5, 0.75, and 1.0, the hysteresis curves of SMA wires and the friction damper and the sum of these two are determined as the hysteresis curve of the PHFD damper. The allowable maximum displacement is assumed to be 50 mm. The loading protocol has an initial value of 5 mm and it

increases by 5 mm after each of the three cycles to break the strips. The ultimate loading limit of displacement controlled is 50 mm (Figure 3).

RESULTS AND DISCUSSION

Analytical models comprised of two high-rise, 18- and 22-story RC frames with a 3.80-meter height per floor and five 6-meter bays divided into two groups—with or without the suggested damper—are used to assess the PHFD damper. A unique moment-resistant frame, or SMRF, was created at the life protective capability level and is included in the initial

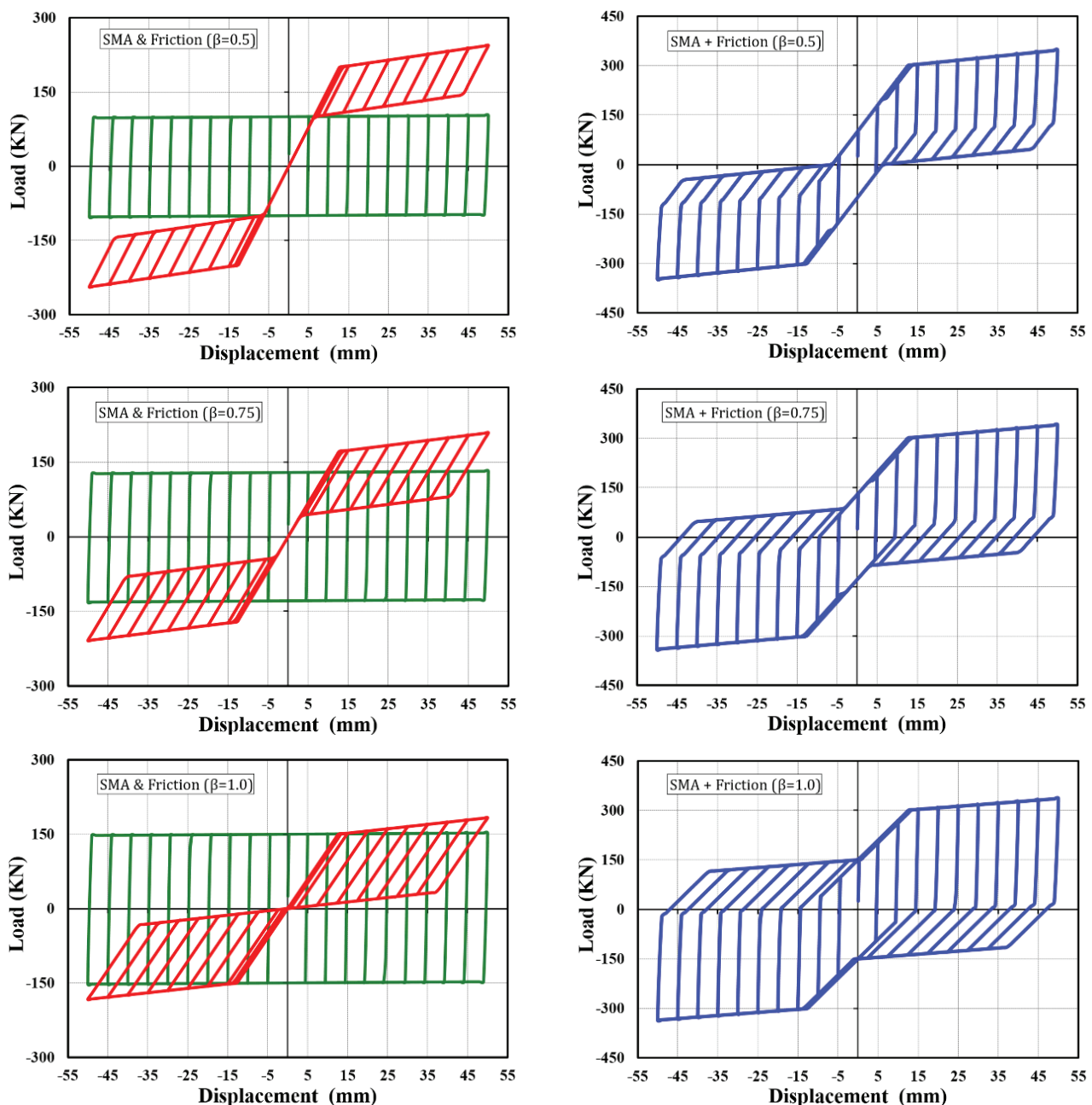


Figure 3. Hysteresis curve of the proposed damper designed with the proposed method for different β values

Table 2. The beam and column members' design requirements for the concrete sections

Section	Height (mm)	Width (mm)	Reinforcement*	
			Top Steel	Bottom Steel
B50x50	500	500	4φ25	3φ20
B50x60	500	600	4φ25	3φ25
B50x65	500	650	5φ25	4φ25
B50x70	500	700	6φ25	4φ25
C50	500	500	20φ20	
C55	550	550	24φ22	
C60	600	600	24φ25	
C65	650	650	24φ25	
C70	700	700	24φ28	
C75	750	750	24φ28	
C80	800	800	28φ28	
C85	850	850	32φ28	

* Reinforcements φ Diameter number (in millimeters)

set of models, as per the most recent version of the Iranian National Building Code and the earthquake standard. The second set of models uses the design methodology proposed in this study to construct a hybrid damper known as PHFD, which is composed of RC frames. The models' tangible parts were created by ACI 318 [22] and IBC [23] requirements. In addition, steel rebars with an elasticity modulus equivalent to that of cement-based concrete with a modulus of elasticity and compression strength are employed in the frames. Design live load and dead load values are deemed to coincide with frames that are subject to gravity loads. The frame mass is determined by taking into account the live load and the dead weight of all components, both non-structural and structural, by the ASCE 41-06 standard [24]. In Table 2, the frames' structural features are displayed. Furthermore, displayed in Figure 4 is the models' elevation.

Considering that the PHFD damper members are yielding, the non-yield members are introduced. A factor of 1.25 R_y is used in their construction, which is comparable to the design of EBF in AISC341 [25]. R_y represents the ratio between the stress at which the projected yield occurs and the stress at which the lowest yield occurs. In the unstable buckling region of the compression bracing, both the compression and tensile forces are double the buckling load (P_b). To avoid unstable buckling of the compression braces, the shear necessary to construct the proposed hybrid friction dampers must exceed the total buckling loads of both braces' horizontal components, multiplied by 1.25 R_y . AISC 341 [25] states that the R_y value of the plate-made pieces is 1.15. Consequently:

$$2P_b \cos\alpha \geq 1.25 R_y V \quad (9)$$

The angle α between the brace and the horizon is given in Eq. (9). $l(P)_b = \text{Eq. (10)}$ may be found using Eq. (9) in terms of the braces' buckling strength.

$$P_b = \frac{1.25 R_y V}{2\cos\alpha} \quad (10)$$

The braces are selected to have a computed buckling capacity minimum (P_b). For all models, certain bracings with a 2UNP120 section and a 996 kN buckling strength are responsive.

The suggested design procedure of the frame of RC with the PHFD damper

The 2D modeling application OpenSee [26] was utilized to create numerical models of the frames. To model the P-delta effects, a vertical column was attached to the frame under the influence of a gravitational force. The axial column modeling incorporates an elastic beam-column component that is specifically constructed with an inertia moment and substantial cross-section. This design is intended to accurately consider the impact of gravity columns on the total response of the frame. To prevent any major moments from being carried by the gravity column, the beam-column parts are linked to one another by rotating springs with extremely little rotational stiffness. At last, the frame and the gravity column are joined by rather stiff truss components. Fixed and pinned are the initial story columns for the frame and gravity column at the base level.

To replicate a stiff diaphragm, every node of a particular floor is limited to its displacement in a horizontal plane. Every floor's seismic mass is split evenly among the beam-column nodes. To ensure that the P-delta impact is accounted for in the frame, gravity loads or direct loading is utilized to the beam-column nodes and the gravity column. The software utilizes a Rayleigh command to specify the damping used for the elements and nodes. To replicate the rotating connection at the intersection of the braces

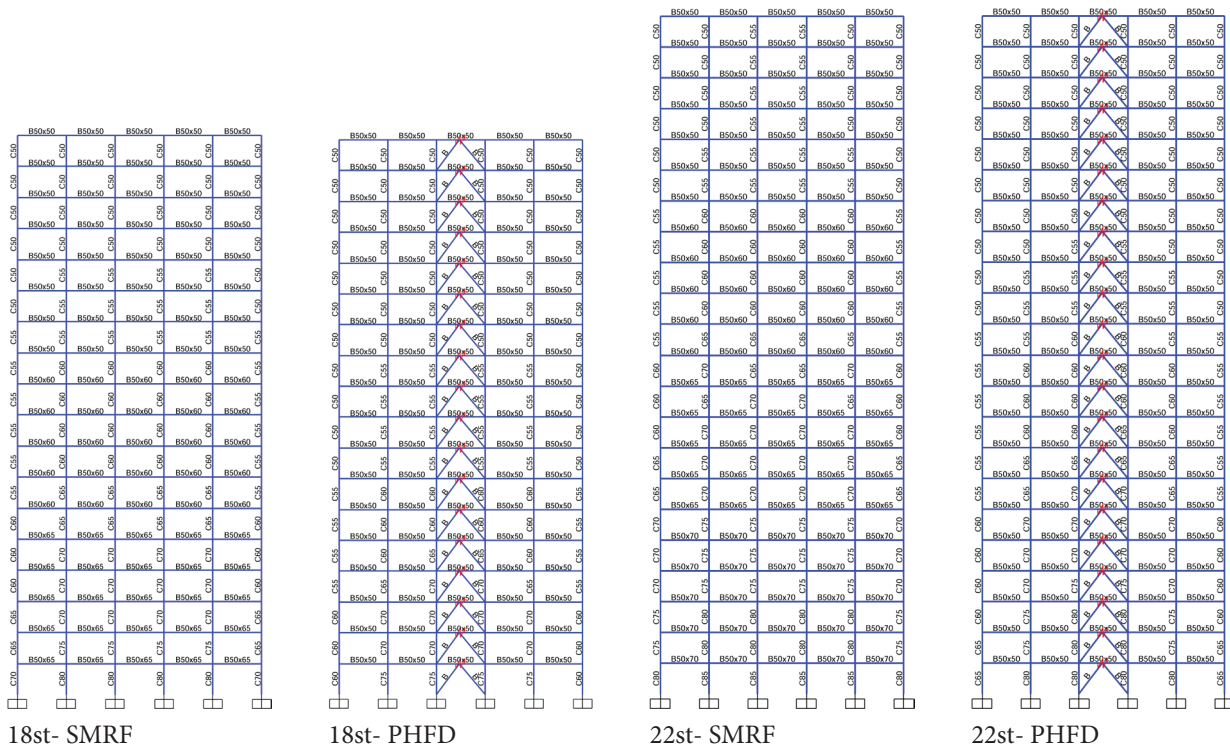


Figure 4. Design details of the concrete columns and beam of the employed models

with the column and beam, a single zero-length element with high stiffness is used solely in the transmission direction. The materials employed are based on the uniaxial material model, which considers the interaction between moment and axial forces and provides a one-dimensional stress-strain relationship. The OpenSees software defines the Concrete02 type confined and unrestricted concrete material model as well as the Steel02 type steel model. Five components comprise the nonlinear beam-column element with extensive plasticity that has been used to represent the beam, columns, and brace members. The foundation for the quartet of integral points in the element direction is provided by the law of Gauss-Lobatto. The fiber model was used to model all segments. According to FEMAP696 [27], nonlinear evaluations were carried out for concrete beams and columns, using flexural cracking coefficients of 0.5 and 0.7. To accomplish this, two concrete materials were specified for the column and beam, with moduli of elasticity multiplied by 0.5 and 0.7.

The SMA wires numerical model was described by materials with uniaxial self-centering capabilities. This material, which resembles a flag, may be used to describe the superelastic behavior of an alloy with shape memory at a fixed temperature. Friction damper models are made using Steel01 materials that have hardening values near zero, which correspond to the elastic-perfectly plastic model. Uniaxial parallel materials are coupled with the aforementioned materials to simulate each component of the PHFD damper and enable simultaneous operation. A

zero-length element is then added to the simulation, placed beneath the concrete beam and above the Chevron brace.

Nonlinear time history analysis

In this part, the seismic behavior of models with and without a PHFD damper in response to earthquake vibrations is investigated. The objectives of this investigation are to examine narrative drift, energy dissipation, and ductility variations. In light of an abundance of nonlinear time history data, nonlinear equations are solved by the MUMPS (multi-frontal massively parallel sparse direct solver) technique (OpenSees), which is part of the OpenSees program and its parallel computing engine. The MUMPS approach is quite effective in earlier studies and can solve large nonlinear equations significantly more rapidly. Chopra [28] states that all investigations have used Newmark’s integration technique [29], which shows strong computational stability of the equations even in areas with extremely non-linear structural behavior. The FEMA-P695 paper serves as the standard for nonlinear time history assessment. This paper states that the gravity load combination that should be applied to structures during analysis is $1.05D + 0.25L$, where D stands for dead load and L for live load. The loading is based on FEMA-P695 [27], which is based on ASCE/SEI 41-06 standards [24].

Ten standardized far-field (FF)-type records—which are available in the FEMA-P695 [27]—have been utilized in this work for non-linear time history analysis (NLTH). Earthquakes in the far field were detected at a distance

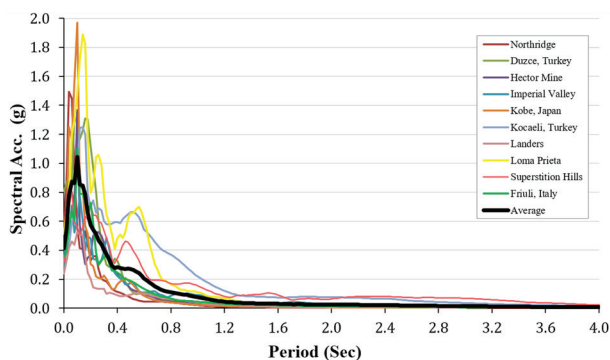
Table 3. The characteristics of used acceleration

ID No.	Record ID	Name	Year	M (Richter)	PGA (m/s ²)	EQ. Scale Factor							
						22 Story				18 Story			
						PHFD		SMRF		PHFD		SMRF	
						CP	LS	CP	LS	CP	LS	CP	LS
1	953	Northridge	1974	6.7	0.52	30.8	20.6	40.8	27.2	25.2	16.8	35.1	23.4
2	1602	Duzce, Turkey	1999	7.1	0.82	12.1	8.1	16.1	10.7	9.9	6.6	13.8	9.2
3	1787	Hector Mine	1999	7.1	0.34	18.6	12.4	24.6	16.4	15.2	10.2	21.2	14.1
4	169	Imperial Valley	1979	6.5	0.35	22.0	14.7	29.1	19.4	18.0	12.0	25.0	16.7
5	1111	Kobe, Japan	1995	6.9	0.51	20.8	13.9	27.5	18.4	17.0	11.4	23.7	15.8
6	1158	Kocaeli, Turkey	1999	7.5	0.36	8.0	5.3	10.5	7.0	6.5	4.4	9.1	6.0
7	900	Landers	1992	7.3	0.24	27.6	18.4	36.5	24.3	22.6	15.1	31.4	20.9
8	752	Loma Prieta	1989	6.9	0.53	11.3	7.5	14.9	9.9	9.2	6.1	12.8	8.5
9	721	Superstition Hills	1987	6.5	0.36	19.4	12.9	25.7	17.1	15.9	10.6	22.1	14.7
10	125	Friuli, Italy	1976	6.5	0.35	19.4	12.9	25.6	17.1	15.9	10.6	22.0	14.7

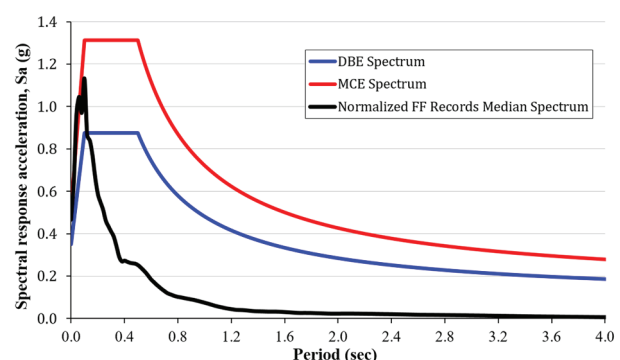
of at least 10 km from the epicenter. Every earthquake is considered a powerful earthquake event if it has a magnitude greater than 6.5 or a PGA of 0.2, and these statistics are gathered from the PEER database. Strong-magnitude earthquakes with extended periods of shaking are selected because they are significant for building collapse and provide prolonged shaking of the structure, both of which are critical for determining overturning safety. The record parameters are displayed in Table 3.

The PHFD damper is tested at two different performance levels. The first performance level is LS (life safety) and prompt repairs of the fuse members that succumbed under the 10% incidence rate of earthquakes every 50 years after entering the inelastic phase, while the major structural parts are still in the elastic phase. To meet this performance goal, the building must instantly resume functioning when the fuse members are replaced. The fuse system’s primary

function is to prevent the original structure’s members from surrendering. In the case of an earthquake with a 2% incidence rate over 50 years, all structural elements are permitted to enter the inelastic phase under the second efficiency level, known as collapse prevention (CP). Two-thirds (2/3) of the seismic risk spectrum at the highest evaluated earthquake (MCE) level should be included in the design earthquake spectrum, according to ASCE7-10, which addresses the minimum design loads for buildings. As a result, the DBE (design basis earthquake) from Iran’s 2800 earthquake standard—which has the same efficiency grade as LS—may be extracted, and its corresponding CP performance level, the MCE-level risk of earthquakes spectrum, may be calculated by multiplying 3/2). Figure 5 shows the normalized seismic spectrum, mean, and the 5% damping DBE and MCE spectra.



(a)



(b)

Figure 5. The first graph (a) shows the earthquake spectrum that has been standardized and includes the average and 5% damping. The second graph (b) shows the average of the standardized earthquake spectrum, as well as the MCE and DBE spectra, all with 5% damping.

To eliminate the anticipated variations in the demand spectrum caused by earthquake motions, earthquakes are adjusted to match the acceleration of the target spectrum at a given code-defined period (T). To do this, every record is adjusted based on the PGV (peak ground velocity), as advised in the FEMA-P695 guidelines. This means that each record's PGV value needs to be normalized. The aggregate spectral acceleration of the recordings is matched to the maximum seismic response spectrum taken into consideration in compliance with the specified code. The scale coefficients of the ten chosen earthquakes are shown in Table 3 for the models at the CP and LS performance levels.

This is a thorough investigation of OpenSees' two-dimensional dynamic nonlinear time history analysis, which was done to determine the two modes of high-rise RC frames with 18 and 22 stories' seismic behavior: (1) designed using the most recent Codes approach, and (2) using the method of PBPD in conjunction with the damper of PHFD. The RDR (residual drift ratio) and IDR (inter-story drift ratio) for each story are the two generally used metrics that are the topic of this study. This makes it possible to assess a building's seismic stability during an earthquake and to specify and analyze the stories with the greatest IDR and RDR. The IDR is utilized to describe the total stability of RC frames during earthquakes. Furthermore, the two aforementioned numbers may be utilized to compute an accurate assessment of the damage that seismic loading has caused to both non-structural and structural components.

Ten earthquakes are originally applied on the frames. These earthquakes match the MCE-level earthquake excitations (probability of 10%) and the DBE-level earthquake excitations (chance of 2% over 50 years). The non-linear time history (NLTH) study of 10 earthquakes yielded the maximum IDR and the average values for the 18 and 22-story frames without and with the PHFD dampers, which are displayed in Figure 6 to evaluate each effectiveness level. At both efficiency levels, the frames fitted with PHFD dampers are more responsive than the traditional frames. Furthermore, it reacts to all of the chosen earthquakes with a much more stable reaction—that is, a more consistent or equal reaction—regardless of the earthquake parameters (such as content frequency) employed in the research. In traditional frames (SMRF), drift distribution happens unevenly at the structure's height, with the strongest IDR happening in the higher stories because of the earthquake's whipping force. This is because RC frames are traditionally designed with the assumption that lower story beams and, in particular, lower story columns, have weaker sections as a result of reduced gravity loads. Thus, the end stories with the largest IDR put the buildings at risk of rupturing in earthquakes and when higher modes predominate at the highest degrees of structural deformation. However, because the PBPD develops the PHFD damper, all stories have a chance to lessen the earthquake's lateral impact. The maximum IDR shift for these models is from the base story

to the third floor and then down to the roof. This suggests that the IDR values become closer together as we approach the roof and that the numbers nearly equalize from the structure's midway point to the top. This outcome demonstrates that the design takes into account the impacts of the interaction using the suggested method and is according to how effectively the RC frame functions with the damper of PHFD. Consequently, a system for resisting lateral loads during seismic events is designed to work almost optimally.

The average value of the maximum IDR (inter-story drift ratio) in frames equipped with passive hybrid friction dampers (PHFD) has shown a more uniform distribution at different floor levels and a notable reduction in the different degrees of damage compared to the principal frame. When comparing the mean maximum IDR of the 18 and 22-story frames at different levels to the main case, the case with a PHFD damper had lower mean maximum IDRs by 69.8% and 57.9%, respectively, at the LS performance level and by 67.7% and 56.6% at the CP level. (21). The mean of the highest IDR decreases as the models' number of tales increases from 18 to 22. Furthermore, the lowering of the maximum IDR mean reduces little when earthquake strength increases from the DBE to the MCE level, which may be disregarded. It is known that utilizing RC frames with PHFD dampers may lower the maximum IDR mean by around 55-70%, irrespective of the number of seismic and story intensities. The aforementioned result demonstrates how a large elastic hardness SMA wire set, big flange-shaped hysteresis loop friction dampers, and large and stable hysteresis loop friction dampers worked together to enable the huge lateral force absorption by the PHFD damper. These components made it possible to design a system with substantial force absorption and lateral rigidity.

In this part, the ratio of RDR of RC frames with PHFD damper is compared with conventional RC frames. As previously stated, one of the innovations in the proposed design approach of the PHFD damper is to determine the optimal number of SMA wires that can have the highest effect in providing a reversible capacity for the structure, along with having a suitable mechanism with friction damper to dissipate a large portion of the seismic forces applied to the structure. Figure 7 reveals the maximum RDR with their mean value for 18 and 22-story frames without and with the PHFD damper derived from the non-linear time history (NLTH) analysis of 10 earthquakes to study the self-centering capacity of the models. As it is clear from the figure, all models with PHFD damper at both LS and CP performance levels have an RDR ratio of approximately zero, with a completely uniform distribution at the structural height. The two main reasons for this result are (1) a significant decrease in the maximum IDR and its uniform distribution in the height due to the use of the proposed design method; (2) the design of the SMA wire set with a special look at its self-centering property, and with the consideration of the SMA forward transformation yield strain (ϵ_M^S) in a mechanism with friction damper in the proposed design method.

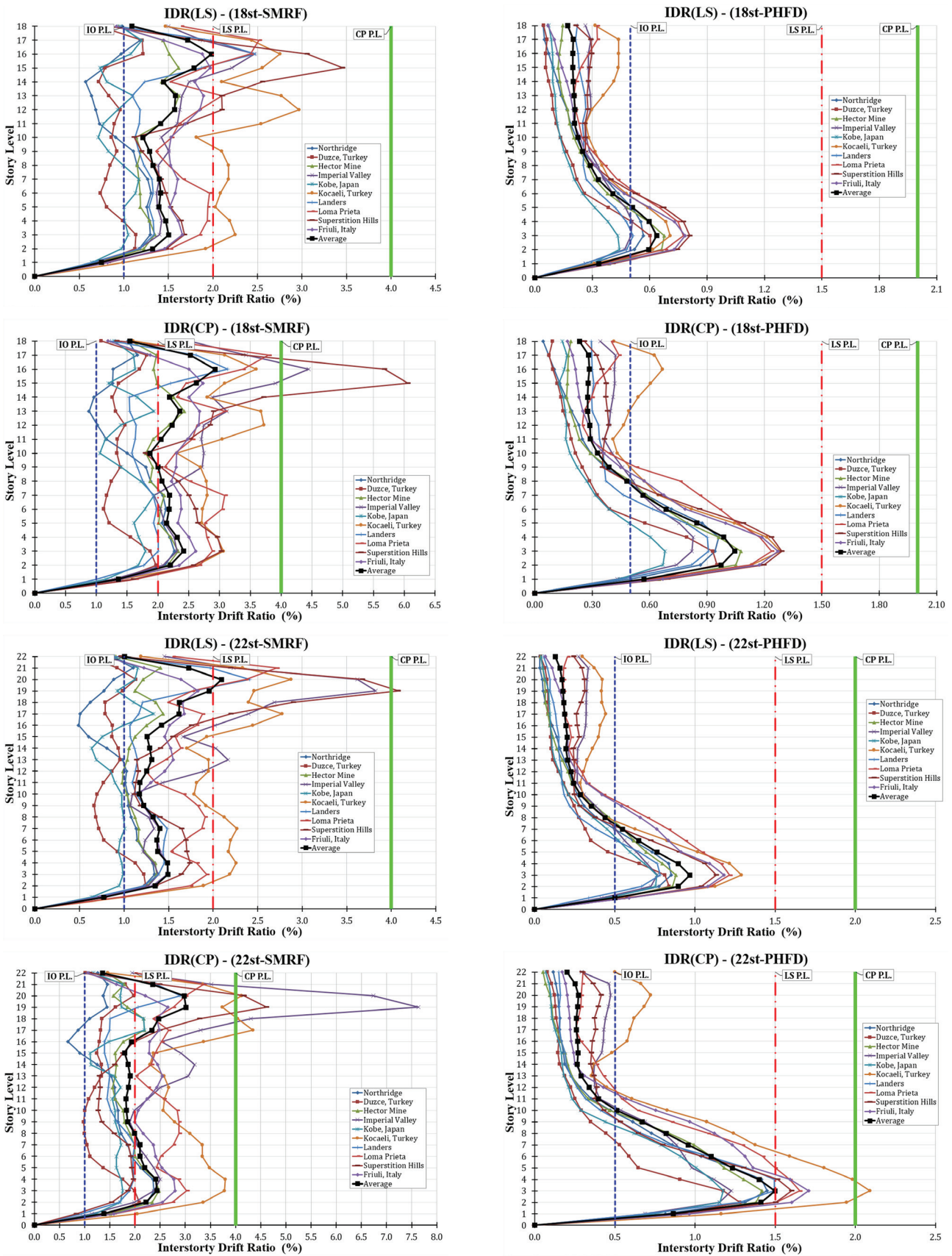


Figure 6. The study examines the efficiency compared between eccentrically braced frames, both with and without PHFD dampers, based on the Interstory Drift Ratio (IDR) at the CP (Collapse Prevention) and LS (Life Safety) performance levels.

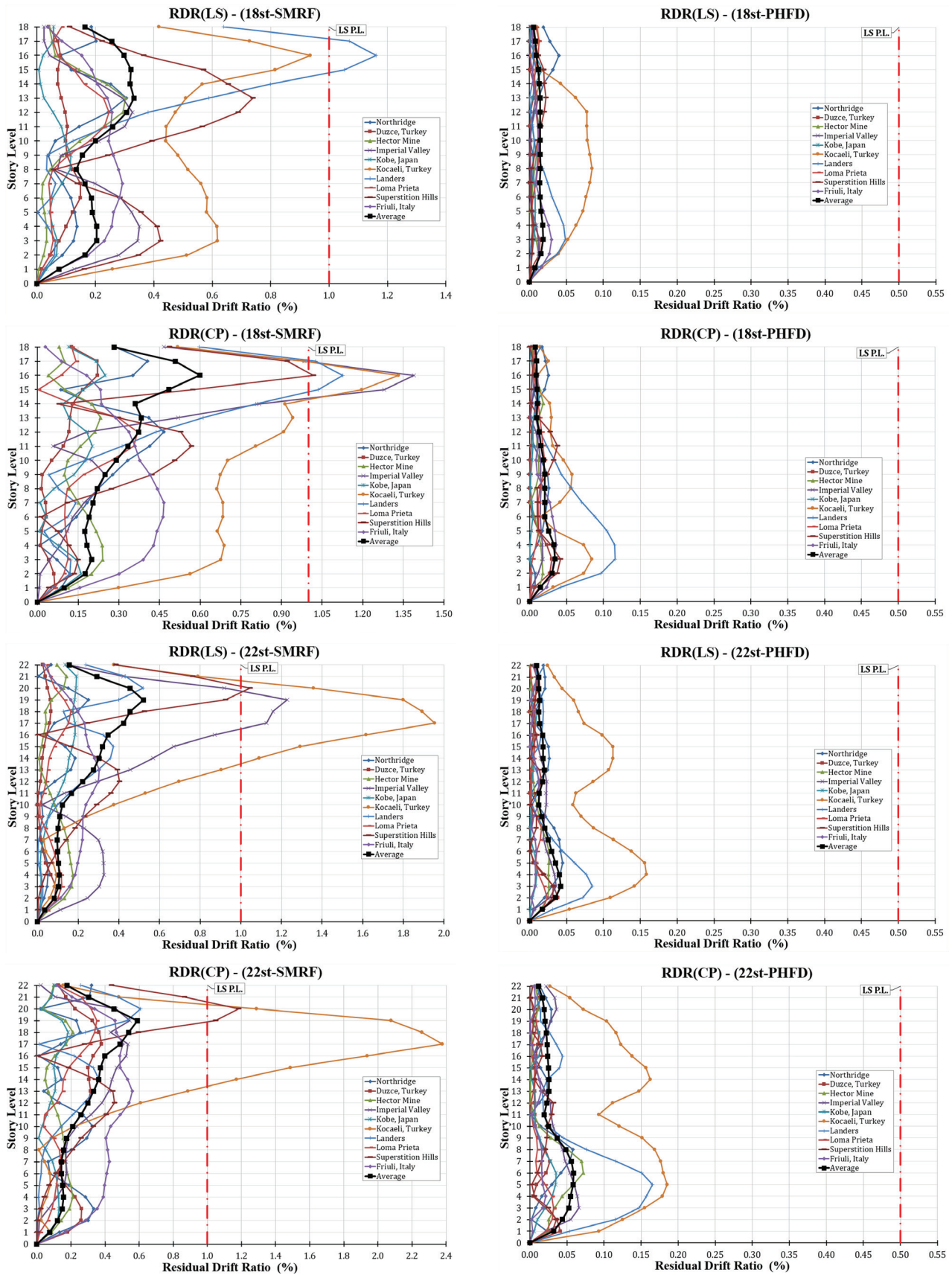


Figure 7. The study aims to compare the performance of the eccentrically braced frame without and with a PHFD damper about the RDR (residual drift ratio) at the CP (collapse prevention) and LS (life safety) performance levels. However, in conventional RC frames, the RDR ratio with a completely non-uniform distribution at the structural

height, although it is acceptable at the performance level, in terms of using the building after the earthquake and counteracting future earthquakes, puts the building in a bad situation. Also, in conventional RC frames, precisely at the location of changing of columns and beam dimensions at the height of the structure, significant growth can be observed at the maximum RDR, particularly in higher stories of models due to the effect of the whipping force of earthquakes in the high-rise buildings. The authors of this article suggest using the PHFD damper with the proposed design procedure based on the performance to resolve the above-mentioned defects commonly found in common lateral load-resisting systems, especially in conventional RC frames.

According to ASCE 41-06, the models' structural performance was assessed, and Tables 4 and 5 provide a summary of the results. Consideration was given to structural performance based on IDR and RDR. CP (collapse prevention), IO (Instant occupancy), and LS (life safety) are the corresponding structural performance levels when IDR is less than 1.0%, between 1.0-2.0%, and more than 2.0%, and when RDR is 0.0%, between 0.0-1.0%, and more than 1.0%, in SMRF models, according to the ASCE 41-06 standard. The structural performance levels in PHFD models are identical to those in IO, LS, and CP when the IDR is less than 0.5%, between 0.5-1.5%, and more than 1.5%, and when the RDR is 0%, between 0.0-0.5%, and greater than 0.5%. As indicated in Table 4, the 18st-PHFD, 18st-SRMF, 22st-PHFD, and 22st-SRMF models' structural performance levels for

Table 4. The level of structural performance of models subjected to 10 earthquakes for the ratio of IDR

Ground motions	18st-SMRF		18st-PHFD				22st-SMRF				22st-PHFD					
	DBE Level		MCE Level		DBE Level		MCE Level		DBE Level		MCE Level		DBE Level		MCE Level	
	IDR (%)	S.P. level														
Northridge	1.30	LS	2.27	CP	0.57	LS	0.96	LS	1.34	LS	2.37	CP	0.85	LS	1.45	LS
Turkey (Duzce)	1.22	LS	1.97	LS	0.61	LS	0.95	LS	1.24	LS	2.09	CP	0.84	LS	1.28	LS
Hector Mine	1.62	LS	2.42	CP	0.68	LS	1.08	LS	1.44	LS	2.48	CP	0.88	LS	1.42	LS
Imperial Valley	2.47	CP	4.45	CP	0.51	LS	0.83	LS	3.82	CP	7.63	CP	0.77	LS	1.23	LS
Japan (Kobe)	1.20	LS	1.94	LS	0.44	IO	0.68	LS	1.33	LS	2.19	CP	0.76	LS	1.18	LS
Turkey (Kocaeli)	2.97	CP	3.72	CP	0.71	LS	1.28	LS	2.87	CP	4.34	CP	1.29	LS	2.09	CP
Landers	2.47	CP	3.13	CP	0.51	LS	0.91	LS	2.41	CP	2.90	CP	0.78	LS	1.49	LS
Loma Prieta	2.52	CP	3.80	CP	0.78	LS	1.24	LS	2.72	CP	3.37	CP	1.22	LS	1.65	CP
Superstition Hills	3.45	CP	6.06	CP	0.81	LS	1.29	LS	4.07	CP	4.62	CP	1.13	LS	1.60	CP
Italy (Friuli)	1.97	LS	2.73	CP	0.79	LS	1.27	LS	1.83	LS	2.80	CP	1.18	LS	1.71	CP

Table 5. The model's structural performance level under 10 earthquakes for RDR ratio

Ground motions	18st-SMRF		18st-PHFD				22st-SMRF				22st-PHFD					
	DBE Level		MCE Level		DBE Level		MCE Level		DBE Level		MCE Level		DBE Level		MCE Level	
	RDR (%)	S.P. level														
Northridge	0.31	LS	0.47	LS	0.04	LS	0.03	LS	0.25	LS	0.33	LS	0.04	LS	0.06	LS
Turkey (Duzce)	0.15	LS	0.22	LS	0.01	LS	0.03	LS	0.09	LS	0.38	LS	0.04	LS	0.04	LS
Hector Mine	0.30	LS	0.24	LS	0.01	LS	0.02	LS	0.17	LS	0.21	LS	0.03	LS	0.07	LS
Imperial Valley	0.35	LS	1.39	CP	0.01	LS	0.02	LS	1.23	CP	0.54	LS	0.04	LS	0.07	LS
Japan (Kobe)	0.12	LS	0.25	LS	0.02	LS	0.01	LS	0.19	LS	0.18	LS	0.01	LS	0.04	LS
Turkey (Kocaeli)	0.94	LS	1.33	CP	0.08	LS	0.08	LS	1.95	CP	2.38	CP	0.16	LS	0.19	LS
Landers	1.16	CP	1.13	CP	0.05	LS	0.12	LS	0.52	LS	0.61	LS	0.08	LS	0.17	LS
Loma Prieta	0.25	LS	0.37	LS	0.01	LS	0.02	LS	0.16	LS	0.35	LS	0.02	LS	0.03	LS
Superstition Hills	0.74	LS	1.02	CP	0.02	LS	0.04	LS	1.05	CP	1.18	CP	0.03	LS	0.04	LS
Italy (Friuli)	0.29	LS	0.47	LS	0.03	LS	0.04	LS	0.30	LS	0.56	LS	0.01	LS	0.02	LS

the IDR of the DBE seismic level are (LS 50%, CP 50%), (CP 0%, LS 100%), (LS 50%, CP 50%), and (CP 0%, LS 100%), respectively, and for the level of MCE seismic, they are (LS 20%, CP 80%), (CP 0%, LS 100%), (LS 0%, CP 100%), and (LS 60%, CP 40%). It was discovered that whereas frames of RC with PHFD dampers gave 100% of the acceptable structural performance level, standard RC frames at the DBE seismic level only offered 50% of that level. Additionally, for RC frames with and without PHFD dampers, the suitable structural performance level at the seismic level of MCE is equivalent to 0–20% and 60–100%, respectively.

The RDR ratio's structural performance level for the 18st-PHFD, 18st-SRMF, 22st-PHFD, and 22st-SRMF models included (LS 100%, CP 0%), (CP 10%, LS 90%), (CP 0%, LS 100%), and (LS 70%, CP 30%) at the level of DBE seismic, and (LS 100%, CP 0%), (LS 60%, CP 40%), (LS 100%, CP 0%), and (LS 80%, CP 20%) at the level of MCE seismic. For all seismic intensities and models, the RC frames with PHFD dampers achieved 100% of the level of targeted structural performance. However, standard RC frames, despite offering 60–80% and 70–90% of the structural performance at the MCE and DBE seismic levels, respectively, have a residual drift of more than 0.5%, which places the structure in an unfavorable position to handle subsequent earthquakes (Table 5).

CONCLUSION

Using the performance-based plastic design technique, two high-rises, 18- and 22-story reinforced concrete buildings were constructed, either with or without PHFD dampers, to investigate the potential benefits of a hybrid friction damper with SMA wire in decreasing the seismic response of tall reinforced concrete buildings. The RC frames and the PHFD damper's interactions were taken into account during design. The study compared the temporal histories of ten far-field earthquakes with models. The findings revealed a decrease in all major indicators, such as the IDR (inter-story drift ratio) and the RDR (inter-story residual drift ratio). Specifically, the mean IDR of RC frames with PHFD dampers was found to be 55–70% lower compared to conventional RC frames. Additionally, the IDR distribution displayed more consistent behavior at different heights of the frames. The average maximum RDR may be significantly reduced by 82%–97% when using a PHFD damper in RC frames as opposed to conventional RC frames. With consideration for the recommended constraint for SMA wires (strain below six percent to estimate the length and strain comparable to the inverted distortion yield strain for an ideal mechanism with a friction damper), this decrease happens when the design that is the performance technique is applied. RC frames with a PHFD damper not only have the maximum energy dissipation capacity, but they also have a respectable reversibility capacity.

DATA AVAILABILITY STATEMENT

There is no data source for this research. All data are presented directly by graphs. All models, data, and code generated or utilized during the study appear in the submitted article.

AUTHORSHIP CONTRIBUTIONS

Authors equally contributed to this work.

CONFLICT OF INTEREST

The author declared no potential conflicts of interest with respect to the research, authorship, and/or publication of this article.

ETHICS

There are no ethical issues with the publication of this manuscript.

REFERENCES

- [1] Qian H, Li H, Song G. Experimental investigations of building structure with a superelastic shape memory alloy friction damper subject to seismic loads. *Smart Mater Struct* 2016;25:125026. [\[CrossRef\]](#)
- [2] Gao Y, Ren W. Theoretical study on vibration control of symmetric structure with shape memory alloy (SMA)-friction damper. *Open Mech Eng J* 2014;8. [\[CrossRef\]](#)
- [3] Ozbulut OE, Hurlebaus S. Application of an SMA-based hybrid control device to 20-story nonlinear benchmark building. *Earthquake Eng Struct Dyn* 2012;41:1831–1843. [\[CrossRef\]](#)
- [4] McCormick J, Aburano H, Ikenaga M, Nakashima M. Permissible residual deformation levels for building structures considering both safety and human elements. in *Proceedings of the 14th World Conference on Earthquake Engineering*, Seismological Press Beijing Beijing, 2008.
- [5] Meli R, Rosenblueth E. The 1985 Earthquake causes and effects in Mexico City. *Concrete International*, ACI, Detroit, Mich, 1986;8:12.
- [6] Asgarian B, Salari N, Saadati B. Application of intelligent passive devices based on shape memory alloys in seismic control of structures. *Structures* 2016;5:161–169. [\[CrossRef\]](#)
- [7] Dolce M, Cardone D, Marnetto R. Implementation and testing of passive control devices based on shape memory alloys. *Earthquake Eng Struct Dyn* 2000;29:945–968. [\[CrossRef\]](#)
- [8] Dolce M, Cardone D, Ponzo FC, Valente C. Shaking table tests on reinforced concrete frames without and with passive control systems. *Earthquake Eng Struct Dyn* 2005;34:1687–1717. [\[CrossRef\]](#)

- [9] Fanaiea N, Monfared MN. Cyclic behavior of extended end-plate connections with shape memory alloy bolts. *Struct Eng Mech* 2016;60:507–527. [\[CrossRef\]](#)
- [10] McCormick J, DasRoches R, Fugazza D, Auricchio F. Seismic assessment of concentrically braced steel frames with shape memory alloy braces. *J Struct Eng* 2007;133:862–870. [\[CrossRef\]](#)
- [11] Parulekar Y. Seismic response attenuation of structures using shape memory alloy dampers. *Struct Control Health Monit* 2012;19:102–119. [\[CrossRef\]](#)
- [12] Qian H, Li H, Song G, Guo W. Recentring shape memory alloy passive damper for structural vibration control. *Math Problems Eng* 2013;2013:963530. [\[CrossRef\]](#)
- [13] Salari N, Asgarian B. Seismic response of steel braced frames equipped with shape memory alloy-based hybrid devices. *Struct Eng Mech* 2015;53:1031–1049. [\[CrossRef\]](#)
- [14] Salichs J, Hou Z, Noori M. Vibration suppression of structures using passive shape memory alloy energy dissipation devices. *J Intell Mater Syst Struct* 2001;12:671–680. [\[CrossRef\]](#)
- [15] Zhang Y, Zhu S. A shape memory alloy-based reusable hysteretic damper for seismic hazard mitigation. *Smart Mater Struct* 2007;16:1603. [\[CrossRef\]](#)
- [16] Zhang Y, Zhu S. Seismic response control of building structures with superelastic shape memory alloy wire dampers. *J Eng Mech* 2008;134:240–251. [\[CrossRef\]](#)
- [17] Massah SR, Dorvar H. Design and analysis of eccentrically braced steel frames with vertical links using shape memory alloys. *Smart Mater Struct* 2014;23:115015. [\[CrossRef\]](#)
- [18] Shiravand M, Nejad AK, Bayanifar M. Seismic response of RC structures rehabilitated with SMA under near-field earthquakes. *Struct Eng Mech* 2017;63:497–507.
- [19] Yalciner H, Sensoy S, Eren O. Time-dependent seismic performance assessment of a single-degree-of-freedom frame subject to corrosion. *Eng Fail Anal* 2012;19:109–122. [\[CrossRef\]](#)
- [20] Kumbasaroglu A. Effect of anchor bars on seismic behavior of infilled walled frames. *KSCE J Civil Eng* 2020;24:2980–2992. [\[CrossRef\]](#)
- [21] Lee C-H, Kim J, Kim D-H, Ryu J, Ju YK. Numerical and experimental analysis of combined behavior of shear-type friction damper and non-uniform strip damper for multi-level seismic protection. *Eng Struct* 2016;114:75–92. [\[CrossRef\]](#)
- [22] ACI Committee. Building code requirements for structural concrete (ACI 318-08) and commentary. 2008. American Concrete Institute, 2008.
- [23] International Code Council. International building code. International Code Council, Inc.(formerly BOCA, ICBO and SBCCI), 2006;4051.
- [24] ASCE/SEI41-06. Seismic Rehabilitation of Existing Buildings. 2006, American Society of Civil Engineers: Reston, Virginia, USA.
- [25] AISC341-10, Seismic Provisions for Structural Steel Buildings. 2010, American Institute of Steel Construction: Chicago, USA.
- [26] OpenSees, Open System for Earthquake Engineering Simulation. Pacific Earthquake Engineering Research Center, 2015.
- [27] FEMA-P695. Quantification of building seismic performance factors. 2009, Federal Emergency Management Agency: Washington, USA, 2009.
- [28] Chopra AK. Dynamics of Structures: Theory and Applications to Earthquake Engineering. 3rd ed. USA: Prentice-Hall; 2008.
- [29] Newmark, NM, Hall WJ. Earthquake Spectra and Design. Engineering Monographs on Earthquake Criteria. Berkeley, CA: Earthquake Engineering Research Institute; 1982.